Evaluation of surface and near-surface melt characteristics on the Greenland ice sheet using MODIS and QuikSCAT data

Dorothy K. Hall,[1] Son V. Nghiem,[2] Crystal B. Schaaf,[3] Nicolo E. DiGirolamo,[4] and Gregory Neumann[2]

[1] The Greenland ice sheet has been the focus of much attention recently because of increasing melt in response to regional climate warming and can be studied using Moderate Resolution Imaging Spectroradiometer (MODIS) and Quick Scatterometer (QuikSCAT) data. To improve our ability to measure surface melt, we use remote sensing data products to study surface and near-surface melt characteristics of the Greenland ice sheet for the 2007 melt season when record melt extent and runoff occurred. MODIS daily land surface temperature (LST), MODIS daily snow albedo, and a special diurnal melt product derived from QuikSCAT (QS) scatterometer data, are all effective in measuring the evolution of melt on the ice sheet. These daily products, produced from different parts of the electromagnetic spectrum, are sensitive to different geophysical features, though QS- and MODIS-derived melt generally show excellent correspondence when surface melt is present. Values derived from the MODIS daily snow albedo product drop in response to melt and change with apparent grain size changes. For the 2007 melt season, the MODIS LST and QS products detect 766,184 km^2 ± 8% and 862,769 km^2 ± 3% of melt, respectively. The QS product detects about 11% greater melt extent than is detected by the MODIS LST product probably because QS is more sensitive to surface melt and can also see subsurface melt. The consistency of the response of the different products demonstrates unequivocally that physically meaningful melt/freeze boundaries are detected. We have demonstrated that when these products are used together we can improve the precision in mapping surface and near-surface melt extent on the Greenland ice sheet.

1. Introduction

[2] Much of the Arctic has warmed in recent decades [*Serreze et al.*, 2000], and remote sensing technology has been instrumental in quantifying the attendant snow and ice changes. Recently there has been a focus on the Greenland ice sheet because of its importance to sea level rise, and the observations of increasing Arctic surface temperatures over the last few decades [*Box*, 2002; *Wang and Key*, 2005; *Comiso*, 2006], and ice sheet mass loss over the last few years [e.g., *Krabill et al.*, 2004; *Luthcke et al.*, 2006; *Rignot et al.*, 2008]. Melting of the entire Greenland ice sheet would contribute approximately 7 m to sea level [*Gregory*

et al., 2004]. If the climate continues to warm at the current rate, mass loss of the Greenland ice sheet will likely accelerate the rate of sea level rise. Field work and weather station data, especially from automatic weather stations (AWS) [*Steffen and Box*, 2001; *van de Wal et al.*, 2005], have been useful for quantifying air and surface temperature changes, as have remotely sensed data. It is vital to improve our ability to monitor and predict the quantity of meltwater emanating from melting ice on Greenland.

[3] In this work, we blended three daily products derived from two different instruments: the Moderate Resolution Imaging Spectroradiometer (MODIS), and the SeaWinds scatterometer on the QuikSCAT (QS) satellite. The products are MODIS-derived surface albedo, MODIS-derived surface temperature, and QS-derived melt. MODIS products are produced during clear-sky conditions only, while QS melt maps are obtained during all sky conditions. We provide a quantitative comparison of daily melt derived from the various products and discuss the physical basis for melt detection. We also delineate surface and near-surface melt extent, detect incipient melt, and monitor the progression of melt. Results show the initiation, progression, extent

[1]Cryospheric Sciences Branch, NASA Goddard Space Flight Center Greenbelt, Maryland, USA.
[2]Jet Propulsion Laboratory, California Institute of Technology, Pasadena, California, USA.
[3]Department of Geography and Center for Remote Sensing, Boston University, Boston, Massachusetts, USA.
[4]Science Systems and Applications, Inc., Lanham, Maryland, USA.

and cessation of melt for the 2007 melt season which is known to have experienced an unusually large melt extent on the Greenland ice sheet [*Mote*, 2007; *Tedesco*, 2007; *Mernild et al.*, 2009].

2. Background

[4] Increased melt has been measured on the Greenland ice sheet using both microwave data [*Mote and Anderson*, 1995; *Abdalati and Steffen*, 2001; *Steffen et al.*, 2004] and infrared (IR) data [*Wang and Key*, 2003, 2005; *Comiso*, 2006; *Hall et al.*, 2008a]. These studies have largely been accomplished using individual sensors such as the passive microwave instrument on the Scanning Multichannel Microwave Imager (SSM/I), surface temperature data from the Advanced Very High Resolution Radiometer (AVHRR), MODIS and scatterometer data from QS. Mass loss of the ice sheet has also been reported using aircraft and Ice, Clouds, and land Elevation Satellite (ICESat) laser altimetry [*Krabill et al.*, 2004; *Zwally et al.*, 2005], and Gravity Recovery and Climate Experiment (GRACE) data [*Luthcke et al.*, 2006]. *Krabill et al.* [2004] found thinning along the ice sheet margins and some thickening at the higher elevations which has since been confirmed by independent studies using different instruments [see, e.g., *Luthcke et al.*, 2006].

[5] There has also been a great deal of work using satellite remote sensing to measure melt extent [e.g., *Wismann*, 2000; *Abdalati and Steffen*, 2001; *Nghiem et al.*, 2001; *Steffen et al.*, 2004; *Fettweis et al.*, 2007; *Mote*, 2007; *Tedesco*, 2007; *Wang et al.*, 2007; *Hall et al.*, 2008a; *Tedesco et al.*, 2008; *Sharp and Wang*, 2009], clear-sky surface temperature [*Stroeve and Steffen*, 1998; *Comiso et al.*, 2003; *Comiso*, 2006; *Hall et al.*, 2008a, 2008b], and albedo [*Nolin and Stroeve*, 1997; *Stroeve et al.*, 1996, 1997, 2005, 2006; *Nolin and Payne*, 2007], and changes in melt-related surface characteristics of the Greenland ice sheet. Specifically regarding the 2007 melt season, *Mote* [2007] showed that there were large areas of anomalously high melt frequency in the summer of 2007, south of 70°N, and *Hall et al.* [2008a] showed that some drainage basins are experiencing earlier melt initiation in southern Greenland. Some details of the algorithms and products used in this work follow.

3. Theoretical Considerations
3.1. Emissivity and Land Surface Temperature

[6] Emissivity is an intrinsic property of the surface and is independent of the temperature. (See *Hook et al.* [2007] for further discussion.) The surface emissivity is defined as the ratio of the actual radiance emitted by a given surface to that emitted by a perfect radiator at the same kinetic temperature. *Salisbury et al.* [1994] show that snow emissivity departs significantly from perfect radiator behavior in the $8-14$ μm part of the spectrum. Emissivity of snow varies with liquid water content and snow grain size especially at larger grain sizes [*Salisbury et al.*, 1994; *Wald*, 1994; *Hori et al.*, 2006]. To obtain snow or ice land surface temperature (LST) with an accuracy of 0.1°C, the emissivity must be known to within 0.1% [*Stroeve et al.*, 1996].

3.2. Albedo

[7] Snow has a very high reflectance in the visible (VIS) wavelengths ($0.4-0.7$ μm), up to nearly 100% at the shortest visible wavelengths, but a much lower reflectance in the near-IR (NIR) ($0.7-2.5$ μm) and short-wave IR (SWIR) wavelengths, even near zero around 1.6 μm. In the NIR, snow is very sensitive to grain size changes, thus albedo decreases when grain size increases [*Choudhury and Chang*, 1979], and melting enhances grain growth [*Dozier et al.*, 1981]. In fact, broadband snow albedo can decrease by >25% within a few days after grain growth begins [*Nolin and Liang*, 2000].

3.3. Scatterometry

[8] A scatterometer is a stable and accurate radar. It transmits electromagnetic waves toward a target and measures backscatter, characterizing the scattering of the waves by the target back to the radar. The snow scattering physics have been modeled by a number of researchers [e.g., *Tsang et al.*, 1985; *Ulaby et al.*, 1981; *Nghiem et al.*, 1995]. With a wavelength of 2.24 cm in free space (corresponding to a Ku-band frequency of 13.4 GHz), QS backscatter is highly sensitive to snow wetness, allowing Ku-band backscatter to be used for snowmelt detection [*Nghiem and Tsai*, 2001; *Nghiem et al.*, 2001].

[9] This is because, in wet snow, liquid water (no salinity) has an imaginary part of about 38 ε_0, approximately 19,000 times larger than that of nonmelting ice [*Klein and Swift*, 1977, *Tiuri et al.*, 1984]. Furthermore, the large difference in the imaginary part of the permittivity of dry and wet snow signifies that Ku-band waves can effectively penetrate the surface layer of refrozen snow to detect subsurface wet snow due to an internal snow temperature profile that has not yet reached the freezing point.

4. Data Products From MODIS and QuikSCAT
4.1. Instruments

[10] MODIS is a 36-channel, polar-orbiting, across-track scanning spectroradiometer that images all areas on Earth every $1-2$ days [*Barnes et al.*, 1998]. The first MODIS was launched on the Terra satellite in December 1999 and the second MODIS was launched on the Aqua satellite in May 2002. The MODIS instruments have seven spectral bands in the $0.4-2.5$ μm range that are relevant for calculation of spectral albedo at either 250- or 500-m spatial resolution. IR channels 31 and 32 (Table 1), are used to calculate daily LST at 1-km spatial resolution.

[11] The SeaWinds scatterometer aboard the QS satellite was launched in June 1999 and has been collecting backscatter data over a swath of 1400 km for the horizontal polarization (H) and 1800 km for the vertical polarization (V). QS acquires backscatter data over the entire island of Greenland two times per day. There are two backscatter products in the QS science data set with different spatial resolutions [*Jet Propulsion Laboratory*, 2006]. The "egg" data backscatter product has a resolution of 25 km, and the "slice" data have a subfootprint resolution of about 12 km [*Jet Propulsion Laboratory*, 2006]. The egg data have a higher accuracy and are used in this work for detection and mapping of melt on the ice sheet.

Table 1. MODIS Bands Used in This Work[a]

MODIS Band	Bandwidth (μm)	Product
1	620–670	MOD10A1 and MCD43 (albedo)
2	841–876	MOD10A1 and MCD43 (albedo)
3	459–479	MOD10A1 and MCD43 (albedo)
4	545–565	MOD10A1 and MCD43 (albedo)
5	1230–1250	MOD10A1 and MCD43 (albedo)
6	1628–1652	MOD10A1 and MCD43 (albedo)
7	2105–2155	MOD10A1 and MCD43 (albedo)
31	10.78–11.28	MOD11 (land surface temperature)
32	11.770–12.270	MOD11 (land surface temperature)

[a]Additional bands (not shown) are used in the input products for the products listed; an example is the Moderate Resolution Imaging Spectroradiometer (MODIS) cloud mask (MOD35) which is input to MOD10A1, MCD43, and MOD11.

4.2. Daily MODIS Land Surface Temperature Product

[12] We use the 1-km pixel resolution MODIS LST standard daily product (MOD11A1) of *Wan et al.* [2002] from Collection 5 reprocessing [*Wan*, 2008], which provides surface temperatures over the Earth's land areas under clear-sky conditions. The LSTs over snow and ice are accurate to within ±1°C [*Wan et al.*, 2002; *Hall et al.*, 2008b]. Relative to other satellite LST results from the Advanced Spaceborne Thermal Emission and Reflection Radiometer (ASTER) and Landsat Enhanced Thematic Mapper Plus (ETM+) instruments, *Hall et al.* [2008b] show relative agreement of ±0.5°C. We do not know how the accuracy of the MOD11A1-derived LSTs varies with temperature. For example, is the accuracy higher, lower, or equal at 0° and −20°C over ice and snow? This is an interesting research question that should be pursued. Nevertheless, the ±1°C accuracy reported by *Wan et al.* [2002] seems reasonable at a variety of ice surface LSTs, and may be a conservative accuracy estimate at ice surface LSTs of −15 to 0°C based on work by *Hall et al.* [2008b].

[13] To determine the LST from an instrument that has two IR channels, one must correct for absorption and reemission of radiation by atmospheric gases, predominately water vapor. The "split-window" method is widely used to achieve some correction for atmospheric effects because the measured temperature difference between the two IR channels is proportional to the amount of water vapor in the atmosphere [*Key and Haefliger*, 1992]. To compute the LST to develop the MOD11_L2 product, the emissivity must be prescribed. (MOD11_L2 is a Level 2 swath product.) For bands 31 and 32, the emissivities used in the algorithm to compute LST over the Greenland ice sheet are 0.993 (for band 31) and 0.990 (for band 32), and do not vary seasonally nor with viewing angle.

[14] *Wan et al.* [2002] calculated coefficients in the generalized split-window LST algorithm by interpolation on a set of multidimensional look-up tables obtained by linear regression of MODIS simulation data from radiative transfer calculations over a wide range of surface and atmospheric conditions. The following MODIS products are input to the MOD11_L2 LST algorithm: sensor radiance (MOD021km), geolocation (MOD03), cloud mask (MOD35_L2), atmospheric temperature and water vapor (MOD07_L2), land cover (MOD12Q1) and snow cover (MOD10_L2). For this work, a pixel is considered "melt" when the LST ≥ -1°C and this simple binary algorithm constitutes the LST melt "product."

4.3. Albedo Products
4.3.1. MODIS Daily Snow Albedo Standard Product

[15] The MODIS daily snow albedo product is a data layer in the snow cover product, (MOD10A1) [*Hall and Riggs*, 2007; G. A. Riggs et al., *MODIS Snow Products User Guide*, 2006, available at http://modis-snow-ice.gsfc.nasa.gov/sugkc2.html]. The daily snow albedo product was developed by *Klein and Stroeve* [2002], with heritage from the work of *Nolin and Stroeve* [1997], *Stroeve et al.* [1997], and *Liang* [2001]. The product was designed to provide global daily broadband albedo measurements for areas mapped as snow by the MODIS snow algorithm to augment the MODIS 16-day albedo product (MCD43) that currently provides 8-day maps of albedo globally at 500-m resolution [*Schaaf et al.*, 2002] using both Terra and Aqua MODIS data (see section 4.3.2). MOD10A1 provides more frequent, though less robust, albedo maps than does the MCD43 product. We use MOD10A1 for this work instead of MCD43, because MOD10A1 has a higher temporal resolution, and because absolute albedo values are not required.

[16] To develop the MOD10A1 product, snow albedo is only calculated under clear-sky conditions as determined using the MODIS cloud mask, MOD35 [*Ackerman et al.*, 1998; *Platnick et al.*, 2003]. A narrowband or spectral reflectance is calculated for each of the seven MODIS "land" bands (Table 1), then combined into a spectrally integrated broadband albedo. Snow is treated as an anisotropic surface [*Klein and Stroeve*, 2002]. Albedo is calculated using various inputs such as the MODIS surface reflectance product (MOD09), land cover product (MOD12Q1), and a Digital Elevation Model (DEM) [*Klein and Stroeve*, 2002]. Models of the Bidirectional Reflectance Distribution Function (BRDF) of snow are created using the discrete ordinate radiative transfer (DISORT) model of *Stamnes et al.* [1988] to correct for anisotropic scattering effects over nonforested surfaces.

[17] Several validation efforts have shown that the MODIS daily snow albedo products are useful over large, flat areas. *Stroeve et al.* [2006] assessed the accuracy of the MOD10A1 (Terra) and MYD10A1 (Aqua) daily snow albedo products over the Greenland ice sheet. They compared the products with surface albedo measurements on the ice sheet from five AWS during the summer of 2004, and found general agreement of the MODIS measurements with the station data. RMSE for the MOD10A1 was 0.067, and 0.075 for MYD10A1. *Tekeli et al.* [2006] studied the MOD10A1 product in the mountains of the Karasu Basin in the headwaters of the Euphrates River in eastern Turkey, and found that the MOD10A1 product overestimated albedo by ∼10% compared to in situ measurements. Additional work by *Sorman et al.* [2006] showed the MOD10A1 albedo product to be good under conditions of low relief and deep snow cover but results were found to be unreasonable in areas with rugged relief, shallow snow cover and over anisotropic surfaces such as forests that were assumed (in the MODIS daily snow albedo algorithm) to be Lambertian.

4.3.2. The 16-Day MODIS Standard BRDF/Albedo Product

[18] The focus of this paper is on the relative change in albedo in relation to melt characteristics rather than on the absolute value of albedo per se. Thus, the absolute calibra-

tion of the different albedo products is beyond the scope of this paper but we compare the state-of-the-art albedo product from MODIS (MCD43) with MOD10A1, to address the suitability of MOD10A1 for monitoring daily albedo of the ice sheet (also see section 5).

[19] The MODIS BRDF/Albedo product uses all cloud-free, directional surface reflectances (MOD09) available over a 16-day period to retrieve an appropriate form of the RossThickLiSparseReciprocal BRDF model every 8 days at a 500-m resolution [*Lucht and Lewis*, 2000; *Schaaf et al.*, 2002, 2008]. A high-quality retrieval is only possible when sufficient cloud-free observations that adequately sample the viewing hemisphere are available. If only a very limited number of observations can be used, then the algorithm relies on a backup method where static field-based BRDFs are used as a priori information and coupled with the few observations to estimate the albedo. For the present work, we used the black-sky albedo (BSA) product, MCD43C3, which is provided at 0.5° resolution on a latitude/longitude grid. (MCD refers to the MODIS combined Terra and Aqua product.) BSA is directional hemispherical reflectance. Also see http://www-modis.bu.edu/brdf/for further information on the MODIS BRDF/Albedo products.

[20] The accuracy of the 16-day albedo products over snow and ice surfaces has been studied. *Stroeve et al.* [2005] found that the MOD43 albedo product retrieves snow albedo with an average RMSE of 0.07 as compared to the station measurements, which have an RMSE uncertainty of 0.035. *Greuell et al.* [2007] validated the 1-km resolution black-sky MODIS Terra 16-day albedo product, MOD43B3, over a glacier in Svalbard using in situ data. They found that the highest-quality albedo data in MOD43B3 provided an RMSE of 0.04.

[21] In addition to the validation studies discussed earlier, we compared the MOD10A1 products with a daily version of the MODIS BRDF/Albedo standard product (MCD43C3) using the "backup" algorithm approach developed by *Strugnell and Lucht* [2001]. This was done to further assess the accuracy of MOD10A1 for the present study. In general, MOD10A1 gives somewhat higher albedo values than does MCD43B3, especially in northern Greenland, and along the western margin of the ice sheet. The greatest differences in albedo are found in northern Greenland, and range generally from >0.1 to ~0.2 meaning that MOD10A1 provides higher values in those areas [*Hall et al.*, 2009]. Parts of the ice sheet in southern Greenland show slightly higher albedo values in the MCD43B3 product compared to MOD10A1. Though the absolute accuracy of the albedo in MOD10A1 has not been assessed fully with respect to in situ data [*Stroeve et al.*, 2006; *Greuell et al.*, 2007] and MCD43C3 [*Hall et al.*, 2009], the relative accuracy of the MOD10A1 product is excellent over the ice sheet, and the relative accuracy is what is most relevant to this work.

4.3.3. Daily QuikSCAT Melt Special Product

[22] The diurnal difference method was developed by *Nghiem et al.* [2001] to monitor the snowmelt process. The algorithm is based on diurnal backscatter difference, a relative quantity between morning and afternoon measurements in half a day to identify current melt, reduced melt, or refreezing conditions [*Steffen et al.*, 2004; *Nghiem et al.*, 2005]. The QS diurnal algorithm does not require the snow

to be completely refrozen (zero liquid water) in the early morning. QS can detect melt as long as there is a difference in the amount of meltwater in snow between morning and evening, causing a difference in the diurnal backscatter. For the case of light melt when there may be some daytime meltwater that fully refreezes during the night (no meltwater in snow), QS sensitivity for melt detection is maintained due to the large difference, by more than 3 orders of magnitude, in the imaginary part of solid ice and that of liquid water.

[23] The diurnal method is based on the relative backscatter difference and not on absolute backscatter. With this relative difference approach, the advantages include independence from: absolute backscatter for different snow classes and snow conditions; scatterometer long-term gain drift; orbital changes of the satellite; and cross calibration between QS and future satellite scatterometers. It also allows the detection of both snowmelt and refreezing. These advantages are not possible with a melt detection method based on a threshold of absolute backscatter, which is dependent on snow grain size, density, accumulation, and ice layer formation created in previous melt seasons [*Nghiem et al.*, 2005]. Therefore, the use of the absolute backscatter is inherently complicated and may lead to biases and inconsistencies both in space and time.

[24] Regarding data resolution, the QS egg data at 25-km resolution have the highest accuracy (0.2 dB for 3σ) for melt detection, which is better than the slice data at 12-km resolution with a lower accuracy resulting in more melt misclassification. A higher resolution of QS data can also be derived with the deconvolution method, however, it requires that the backscatter remains unchanged in each high-resolution pixel during the period of data acquisition (period of a day to a week depending on the scale of the enhanced resolution) used in the resolution enhancement process as stated by *Early and Long* [2001]. This requirement invalidates the use of QS data at a high resolution obtained by the deconvolution method for snowmelt detection because backscatter can change significantly (by as much as an order of magnitude or more) within a few hours or between ascending and descending passes in half a day when snowmelt occurs [*Nghiem et al.*, 2001, 2005; *Steffen et al.*, 2004]. Furthermore, the deconvolution method also needs the merging of data from both ascending and descending passes to have a sufficient number of data samples to significantly enhance the resolution. In that case, one is forced to use the method based on backscatter threshold, leading to inherent inconsistencies and biases.

[25] We implement here a simple additional step to require that melt occurs at a given pixel in two consecutive days for the pixel to be identified as a melt pixel using QS egg data. This product is called the "QS consistent melt" product (QCM) to distinguish it from the "QS transient melt" product (QTM) when a pixel is classified as melt as long as a transient melt is detected in a single day. Compared to QTM, QCM reduces the inclusion of isolated melt events due to transient weather conditions such as warm air advection associated with storms from the south or warm fronts from the ocean. With the exclusion of transient isolated melt cases, the QCM melt extent is smaller than the corresponding QTM extent. QTM was used to study transient melt events in the dry snow facies of the Greenland ice

sheet in the anomalous melt season of 2002, and the results indicate that such isolated melt events are short-lived and infrequent (∼1 day) [Steffen et al., 2004; Nghiem et al., 2005]. When the difference between QTM and QCM (QTM-QCM) is used, the variability of isolated or transient melt events can be quantified. This can be related to sensible heat advection and synoptic atmospheric dynamics, which is planned for future study. However, for this work, the use of the QCM product is necessary to allow a consistent comparison with the MODIS melt detection algorithm.

5. Methodology

[26] All MODIS and QS data were registered to an Albers conical equal-area projection. Daily (MOD10A1) albedo maps were produced, and the MODIS LST and QS melt product results were blended into a single grid. Using the QS melt product along with the MODIS LST melt product, various categories of melt are provided in the blended maps: (1) no melt, or "snow," either MODIS LST or QS maps (shown as "grey" on the blended maps and called "Both Snow"); (2) melt on both MODIS LST maps and QS (shown as "red" and called "Both Melt"); (3) melt on the MODIS LST map and "Reduced Melt" on the QS map (shown as "orange" and called "MODIS Melt/QS Reduced Melt"); (4) QS-derived refrozen snow (shown as "purple hatched" and called "QS Refrozen Snow"); and (5) snow on MODIS and melt on QS (shown as "blue" and called "MODIS Snow and QS Melt").

[27] "Reduced melt" means that the QS algorithm detects melt, but the rate or intensity of melt is lower compared to the previous day's melt conditions. Since the QS algorithm detects melt based on differing amounts of liquid water in snow (i.e., snow wetness) between morning and afternoon, if there is a smaller diurnal change in backscatter (i.e., less difference in liquid water content) relative to a larger backscatter change (>1 dB) in previous days, it means that there is less daytime heating and thus less melting, and consequently a slower melt rate (which is thus called "Reduced Melt" on the QS melt product).

[28] Transects from west to east were developed to illustrate the location of changes in albedo (from MOD10A1) with respect to the melt categories on the blended maps. Elevation is derived from the DEM of Bamber et al. [2001]. The location (in km) on the x axis in each transect represents number of kilometers from the beginning of the transect, from west to east.

[29] To identify the geophysical meaning of the melt determined by the MODIS-QS composite map, we investigate seasonal melt evolution over various melt regions of the Greenland ice sheet, from incipient through active melt, to freezeup. This approach allows us to tie the MODIS-QS blended melt classes to physical parameters such as elevation, temperature and albedo.

[30] We also analyze maximum melt for the 2007 melt season from MODIS LST and QS, and compare the melt season results from both products on a single map. A map of minimum albedo for the 2007 melt season was also produced, to compare with the combined LST-QS seasonal melt map.

[31] The map of minimum albedo was developed in the following way. First, sharp dips in the albedo were minimized. The sharp albedo dips are generally caused by unmasked clouds, but may also be related to the presence of melt ponds [see Box and Ski, 2007; Sneed and Hamilton, 2007]. Sneed and Hamilton [2007] discuss melt ponds and extensive areas of nonponded surface water. These areas could influence the albedo within the MODIS pixel. To eliminate or minimize inclusion of albedo dips, each pixel value of albedo was compared to pixels from the two previous days of conservatively noncloudy data. If the current day albedo was a new minimum and had a lower value than that of the two previous days by 10 percentage points or more, then it was considered a "dip" and eliminated. If the albedo was lower by less than 10 percentage points for both of the previous two good days, then it was considered an acceptable value, and the current day's albedo was recorded as the lowest albedo value for that pixel.

6. Results

[32] The MODIS daily snow albedo product is the most sensitive of the three products to surface changes. The QS melt product is the most sensitive to surface and near-surface (centimeters to decimeters) melt intensity, and though the MODIS LST product is not sensitive to melt intensity because of the binary nature of the algorithm used for this work, it is still highly effective in detecting active surface melting, and can be used alone, or in conjunction with other data to detect surface melt/freeze boundaries.

6.1. Incipient Melt Phase

[33] Lowering of the albedo on the ice sheet was first seen around 22 March (where the albedo decreased from ∼95% to as low as ∼80% in the southern part of the ice sheet). The LST-QS blended maps do not show sustained melt until late May/early June 2007 (on the periphery of the ice sheet), so it is highly unlikely that the MODIS daily snow albedo algorithm, MOD10A1, was detecting surface melt in March and April especially in the higher-elevation parts of the ice sheet. A likely explanation for the albedo decrease beginning in mid-March is that shadows from sastrugi and other wind-sculpted snow features began to change, causing a reduction in the albedo when the solar zenith angle is high. According to Stroeve et al. [2005], undulations and wind-sculpted features such as sastrugi, represent altered snow grain sizes and introduce shadowing effects to the snow surface that can lower the albedo.

6.2. Active Melt Phase

[34] Melt is often detected first in the QS product and soon after in the MODIS LST. On 1 June 2007, in the southwestern margin of the ice sheet, QS shows extensive melt on the ice sheet margin (red, orange and blue areas on blended map in Figure 1a), with less melt observable in the MODIS LST product. On the next day, 2 June, the extent of melt, as observed in the MODIS LST product, increased (red and orange areas in Figure 1b). By 3 June, both the LST and QS products show extensive melt in the southwestern margin of the ice sheet (Figure 2b). The albedo map (Figure 2a) also indicates melting as evidenced by the
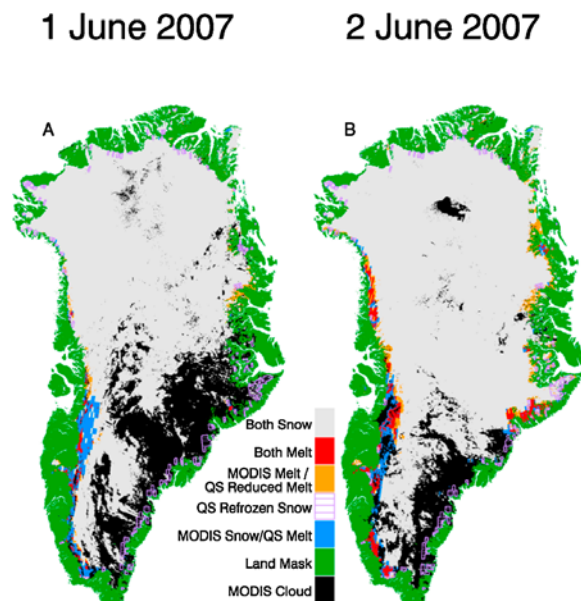
Figure 1. Maps developed from blending MODIS land surface temperature (LST) and QuikSCAT (QS) melt maps from (a) 1 June 2007 and (b) 2 June 2007. Note the melt along the eastern and western margins of the ice sheet.

presence of significantly reduced albedos (<75%) along the southwestern margin of the ice sheet as compared to inland values. Though not shown, a similar pattern is evident for 26–27 June, 1–2 July, and 11–12 August, as well as on other dates, where QS detects melt first, and then the MODIS LST product detects melt after a 1- to 2-day delay. This delay may be caused by one or a combination of three physical reasons: (1) meltwater may be present below a frozen surface; this can be detected only by QS; (2) QS is more sensitive to melt detection than is the MODIS LST; or (3) MODIS may be missing surface melt if it is not mapping the area at the warmest time of the day, while the QS algorithm detects any melt between 0600 and 1800 local time (data at the outer sides of each swath can be earlier or later than the local time of the data acquired at the swath center due to the large swath width).

[35] On 3 June on the eastern part of the ice sheet, the east transect plot (Figure 2c) illustrates a dramatic drop in albedo (from ∼83 to ∼25%) at the snow line from the frozen to the melted parts of the ice sheet surface between ∼42 and 52 km from the beginning of the transect (see change from gray to orange area). The solid black line represents albedo. All of the products respond to a sudden change from a frozen surface to a melted surface from west to east. Note the sharp drop in elevation coincident at this location as well, which is most probably the controlling mechanism for the change in surface state. The dashed black line represents elevation.

[36] Turning to the southwest transect, also on 3 June, we see albedo variability that is likely caused by inhomogeneity in surface melt within the area of melt on the blended map (orange and red areas in transect in Figure 2d). Surface melt features such as melt ponds cause changes in albedo between ∼10 to 91 km from the beginning of the transect. Snow albedo increases from a location on the transect, from

∼24 to 137 km, to a maximum of ∼80%, in response to smaller grain sizes at the higher elevations. Note the somewhat abrupt increase in albedo before 114 km when melted snow as detected by QS (blue) becomes frozen (gray), a likely result of decreased surface snow grain size.

[37] MOD10A1 is sensitive enough to grain size changes so that it can be used to detect conditions associated with different melt intensities. The lowest albedos (<25%) observed in 2007 correspond to bare glacier ice. The QS and MODIS LST melt products do not distinguish bare ice and/ or impurity-rich ice from snow covered ice when the surface is dominated by a wet layer. The distinct albedo zones in southwestern Greenland seen in Figure 2a, and in Figure 3a on 5 July indicate sustained melt features and they correspond with the MODIS LST and QS melt when both show active melting (red on the blended maps in Figure 3b). This is probably an area containing bare ice on 5 July.

[38] On 5 July 2007, a gradual lowering of the albedo is seen in the east transect (Figure 3c) from the zone of snow (gray) where the albedo is ∼85%, to the zone of refrozen snow (purple hatched area over gray) accompanying a grain size increase from frozen snow to refrozen snow. Albedo continues to decrease in the zone of refrozen snow. Then there is a sharp drop in albedo (from ∼75 to 65%) from the zone of refrozen snow to the zone of wet snow/reduced melt (orange) (Figure 3c) at a location of ∼304 km.

[39] Also on 5 July, Figure 3d, a transect in southwestern Greenland, indicates a range of albedos (from ∼<35 to 70%) within the QS-MODIS zone of active melting (red) implying albedo sensitivity to melt intensity (or possibly to impurity-rich ice) whereas the QS and LST melt algorithms simply identify this area as melt. Also in the southwest transect (Figure 3d), albedo rises sharply from an area of melt that is detected by both MODIS and QS (red), to melt detected by QS only (blue) at 84 km where the surface is frozen according to the LST product. The albedo continues to increase, but gradually from melted to refrozen snow (purple hatched over gray) and then to the region of dry snow (gray), again probably in response to smaller grain sizes from melted and refrozen to dry snow where no melt was detected by LST and QS.

[40] By 4 August 2007 (Figures 4a–4c), most of the inland parts of southern Greenland are refrozen (see purple hatched over gray area on Figures 4b and 4c), with neither MODIS LST nor QS indicating active melt except near the ice sheet margins. The transect (Figure 4c) across southern Greenland shows that the albedo is abruptly higher at a location of ∼35 km, moving eastward from melt detected by both MODIS LST and QS (red) where the albedo is as low as ∼30%, to melt detected by QS only (blue) where the albedo rapidly increases to nearly 80%. The MODIS LST and albedo products are consistent here: the large increase in albedo is coincident with the LST product changing from detecting a melted to a frozen surface at ∼35 km. In the region of melt observed by QS only (blue) after 35 km, the albedo changed from a low of ∼30% to a high of ∼78%. The existence of QS subsurface melt is physically consistent with this observation since a refrozen surface can maintain the freezing condition for new snow from either snow drift or snowfall with a higher albedo. The steep elevation increase in this area is likely responsible for changes in surface temperatures and in melt states with different wet-
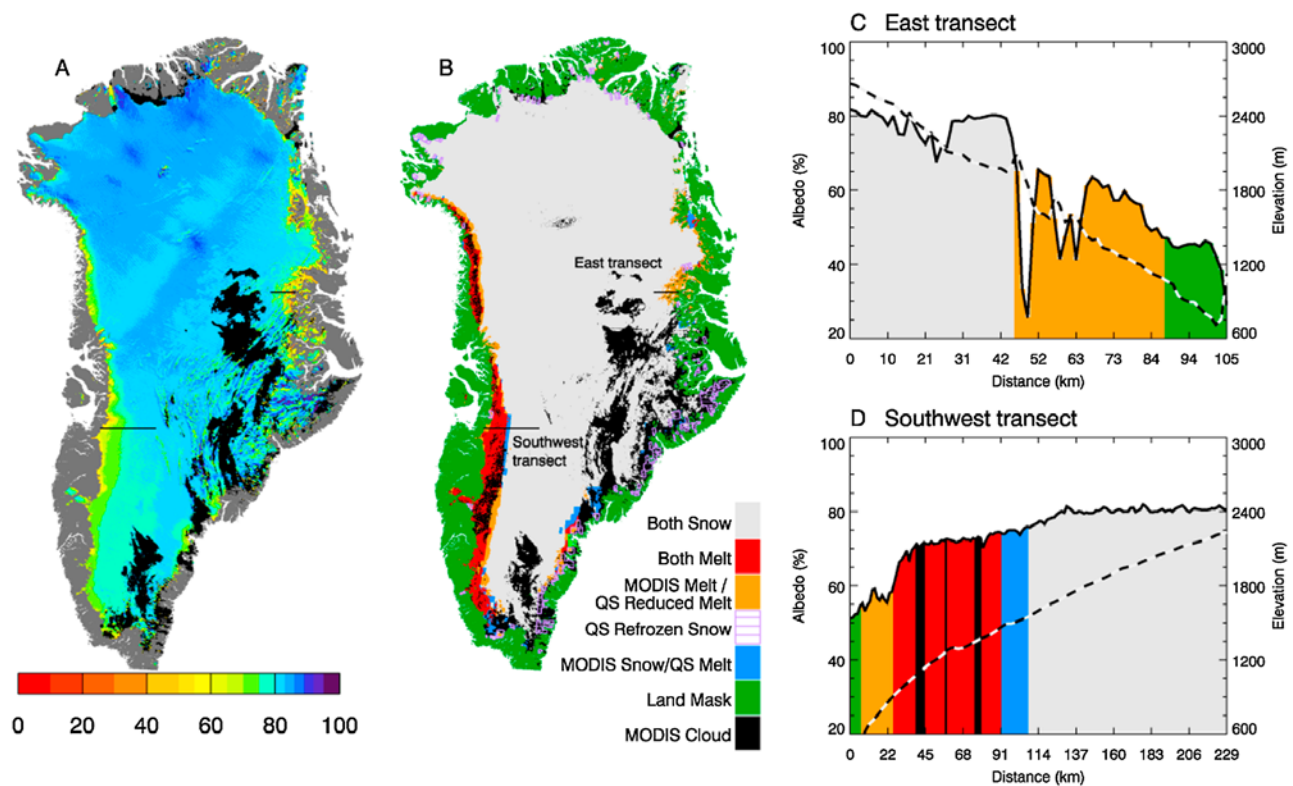
Figure 2. (a) MOD10A1 albedo map from 3 June 2007 illustrating pronounced reduced albedo in the western margin of the Greenland ice sheet corresponding with surface melt. (b) LST−QS blended map from 3 June 2007; the locations of transects in (c) east and (d) southwest are shown as the black lines in Figures 2a and 2b. The locations shown on the vertical axes represent number of kilometers from the start of the transect; note that the horizontal scale is different in Figures 2c and 2d. The MODIS LST and albedo maps, though acquired on the same day, often show different areas of cloud obscuration because the algorithms to produce each daily product may each select different swaths (from different times of the day) and clouds may thus be in different places. Dashed line is elevation; solid line is albedo.

nesses corresponding to the relative changes in albedo. Or, the albedo dip at ∼35 km may signify the presence of impurity-rich ice (J. Box, written communication, 2009).

6.3. Extreme Melt Episode

[41] On 13 August 2007 (Figures 5a–5c) there was a melt event in which active melting is evident on both the LST and QS products (red, orange and blue in southern Greenland in Figure 5b). The MODIS daily snow albedo map, Figure 5a, illustrates lowered albedo in southern Greenland as compared to the previous day, probably due to larger grain sizes resulting from surface melt on 13 August (Figure 6). Albedo along the westernmost part of the transect is shown in Figure 6 for 12 and 13 August, with a lowering of the albedo during the melt event on 13 August. Also on 13 August, extensive melt is observed at the eastern ice sheet margin (red and orange) in Figures 5b and 5c.

[42] A transect extending from west to east across the southern part of the ice sheet is shown in Figure 5c. Steep increases in albedo occur within the melted (red and orange) areas to a maximum of ∼75%, resulting from lowered

surface temperatures (a transition from a melted to a frozen surface) coincident with steeply increasing elevation (see dashed line). Note the abrupt albedo increase when the MODIS LST product indicates a change from a melted to a frozen surface (from the red to blue areas at the location of just before 231 km in Figure 5c). (This was also noted on Figure 3d.) Again, the consistency of the melt states identified by the LST and QS products (from melt (red), to a frozen surface with subsurface melt (blue), to dry snow (gray)), with the albedo product confirms that a geophysical boundary is identified. Both MODIS products are responding to the abrupt change from a wet to a frozen surface while QS continues to detect melt below the surface (blue) or is responding to melt that occurred sometime during that day approximately between 06:00 and 18:00 local time that was missed by the MODIS products that are based on instantaneous "snapshots" in time, of the surface.

[43] *Hanna et al.* [2008] show that the summer of 2007 was the second warmest since 1961, and *Mernild et al.* [2009] show record melt extent and runoff from the ice sheet in 2007. During the summer of 2007, some locations
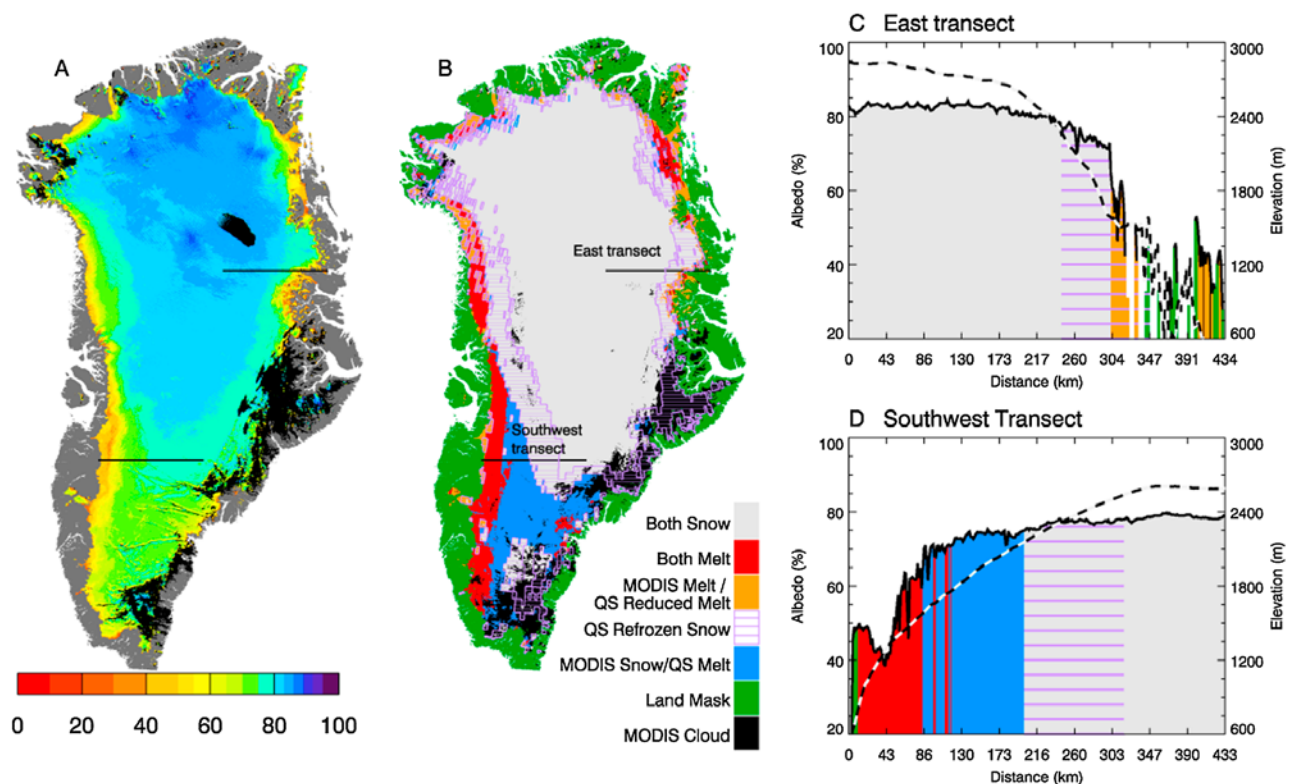
Figure 3. (a) Extensive area of melt in southern Greenland as detected by the MOD10A1 albedo product on 5 July 2007. (b) MODIS LST–QS blended map from 5 July 2007. (c) Transect showing albedos and delineation of melt zones. The locations of transects showing albedos and delineation of melt zones from areas in (c) eastern and (d) southwestern Greenland are shown as the black lines in Figures 3a (east) and 3b (southwest). (White areas in Figure 3d indicate areas where the albedo was <20% or missing.) The MODIS LST and albedo maps, though acquired on the same day, often show different areas of cloud obscuration because the algorithms to produce each daily product may each select different swaths (from different times of the day) and clouds may thus be in different places. Dashed line is elevation; solid line is albedo.

on the ice sheet experienced as many as 50 more days of melt than the 1973–2007 average [*Mote*, 2007]. T. Mote (written communication, 2009) identified an extensive area of melt on 13 August 2007 in southern Greenland using passive microwave data that is roughly comparable in size, though larger, than the melt region identified using the MODIS LST map on that same day. *Tedesco* [2007] also noted an increase in frequency of melt in regions above 2000 m.

6.4. Maximum Melt Extent in 2007 Melt Season

[44] The maximum extent of melt detected by the MODIS LST (766,184 km^2 ± 8%) and QS (862,769 km^2 ± 3%) melt products is shown in Figure 7. MODIS and QS generally agree (89%) in the detection of seasonal melt extent with about 11% larger extent detected by QS. Differences occur at higher elevations farther inland. Melt extent reached higher elevations as measured by QS probably because of the capability of the QS to detect subsurface as well as surface melt. In addition, the peak temperature and melt of

the ice sheet probably occurs at about 1300–1400 local time on most days. The QS diurnal algorithm is based on the presence of melt between 0600 and 1800 local time, which includes the hours of peak melting and MODIS swaths from those hours may not always be selected by the MODIS LST algorithm, or the swath observations (which are instantaneous) at those hours might have been cloud obscured. Thus less melt is likely to be detected by the MODIS LST product when those circumstances prevail.

6.5. Freezeup Phase

[45] By 27 August 2007 (images not shown), the albedo remained low at the ice margin in both eastern and western Greenland (but it is more pronounced in western Greenland because the ablation zone is wider there); in addition, the MODIS LST map indicates that melt was occurring in those locations, while the QS map indicates reduced melt. As snow continued to fall and as temperatures decreased, the albedo increased and the blended map shows increasingly

4 August 2007
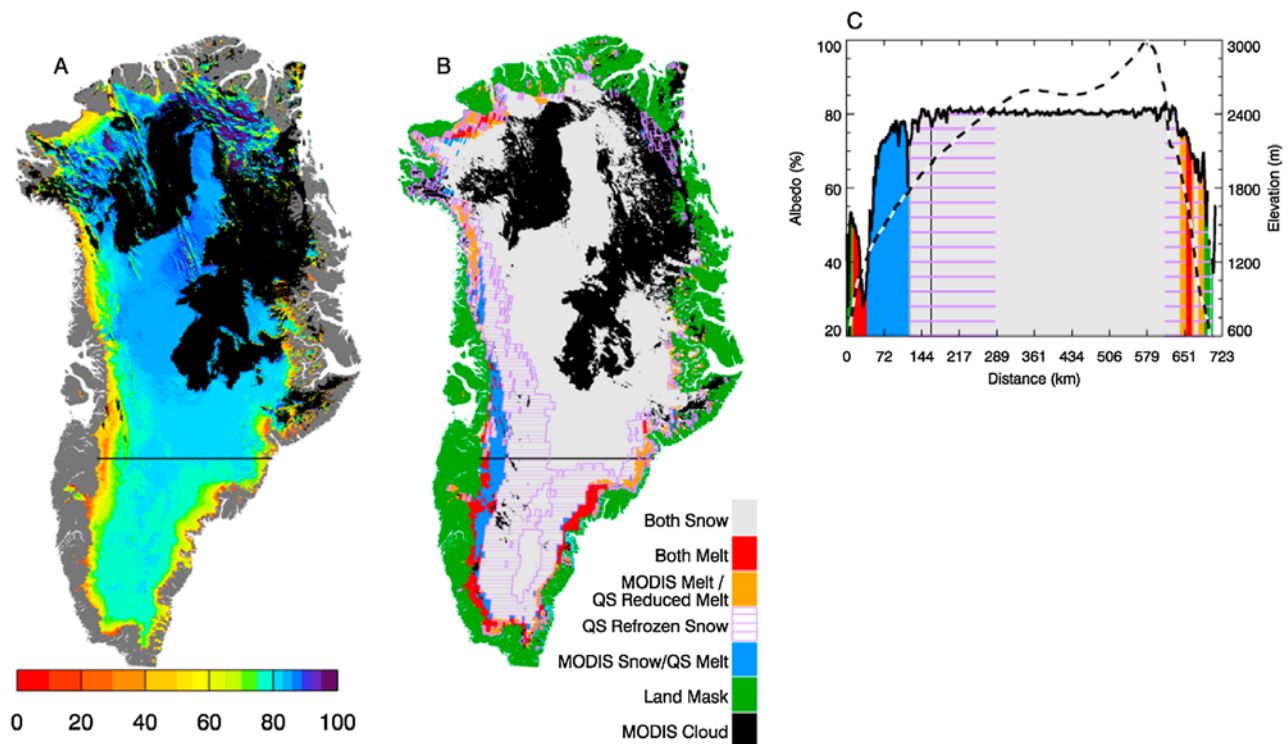
Figure 4. (a) MOD10A1 albedo map from 4 August 2007 showing reduced albedo in refrozen snow area of the southern part of the ice sheet. (b) MODIS LST–QS blended map from 4 August 2007 showing that nearly all of the ice sheet in southern Greenland has refrozen except at the edges of the ice sheet. (c) Transect in southern Greenland. The location of the transect in Figure 4c is shown as the black line in Figures 4a and 4b. The MODIS LST and albedo maps, though acquired on the same day, often show different areas of cloud obscuration because the algorithms to produce each daily product may each select different swaths (from different times of the day) and clouds may thus be in different places. Dashed line is elevation; solid line is albedo.

less melt along the ice margins as the freezeup period progressed.

7. Discussion of Uncertainties

### 7.1. Detection of Subsurface Melt by QuikSCAT

[46] QS indicates significantly more melting in southern Greenland on 5 July 2007 than does MODIS LST as evidenced by the extensive "blue" area in southern Greenland seen on Figure 3b. Analysis of the LSTs in the blue area indicates that there are large areas where the LSTs are −3° and −2°C which is close to the LST threshold for melt used in this work (≥−1°C). First, QS has a greater sensitivity for detecting melt as discussed previously. In addition, the skin depth for the LST product is only a few mm while the QS can penetrate through the refrozen snow of the surface layer. Therefore, it is likely that the surface was frozen over much of the area and that there was internal liquid water content below the surface layer. Further evidence of this can be drawn from the cases where both MODIS products detected a frozen surface while the QS product detected melt (see, for example, the "blue" area in Figure 4c as discussed previously).

[47] *Hoffman et al.* [2008] indicate that subsurface melt is often present in a glacial environment. Moreover, *van den Broeke et al.* [2008] show that radiation penetration can cause the ice to melt below the surface while summer melting can be intermittent due to nighttime surface freezing at higher elevation (and thus farther inland) of the ice sheet. In Figures 2–5, the blue areas (QS melt and MODIS dry snow) are consistently located farther inland at higher latitudes compared to the corresponding red areas (both QS and MODIS melt). This may further explain why melt is detected by QS and not by the MODIS LST.

7.2. Temporal Considerations

[48] Another uncertainty factor is that the LST product may not be acquired at a time of the day when peak melting occurs, while QS senses the meltwater accumulated during the melt process throughout the day between ∼0600 and 1800 local time. In the days after 5 July 2007, much of the blue area in Figure 3b becomes mostly red, indicating the agreement of both MODIS and QS in the identification of melt extent as melt progresses. But if melt does not progress, the two products will not necessarily agree, that is, if the surface does not melt.

13 August 2007
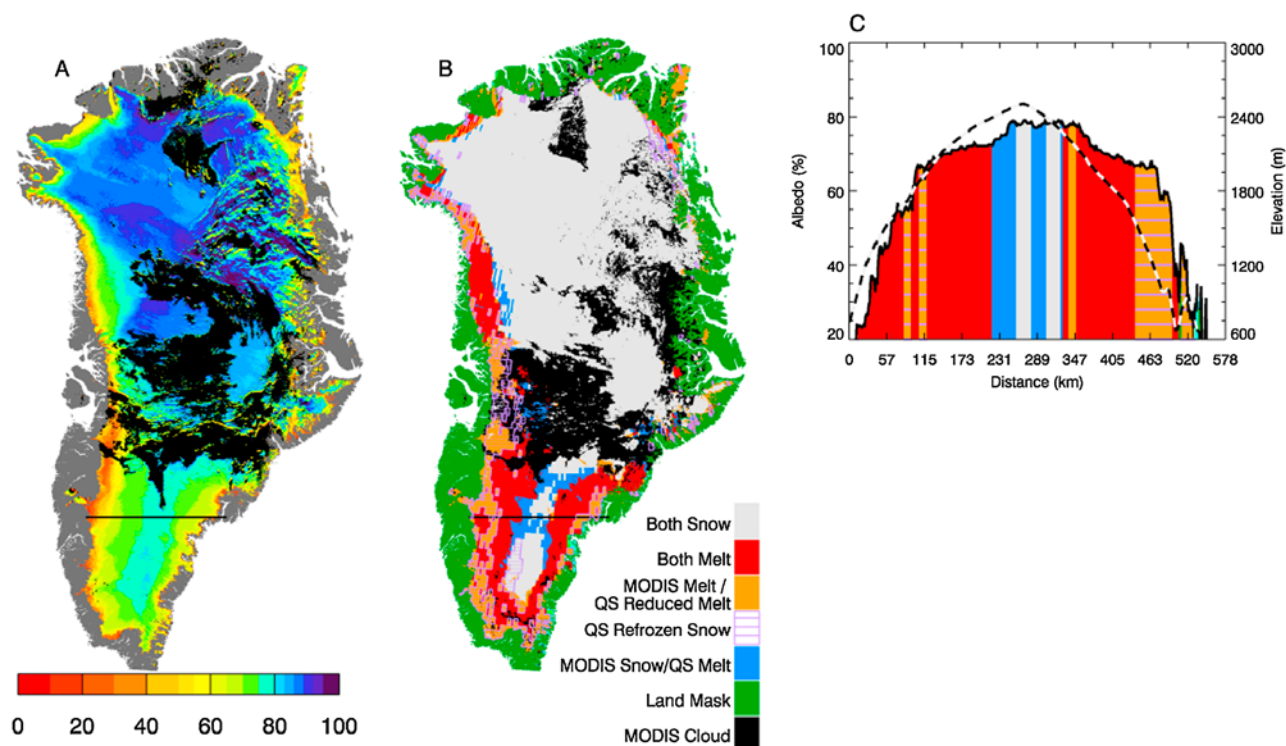
Figure 5. (a) MOD10A1 albedo map from 13 August 2007 showing reduced albedo in refrozen snow area in the southern part of the ice sheet. (b) MODIS LST−QS blended map from 13 August 2007 showing active melt in southern Greenland. (c) The location of the transect across the ice sheet is shown in Figures 5a and 5b. The MODIS LST and albedo maps, though acquired on the same day, often show different areas of cloud obscuration because the algorithms to produce each daily product may each select different swaths (from different times of the day) and clouds may thus be in different places. Dashed line is elevation; solid line is albedo.

7.3. Limitations of the Daily Snow Albedo Product

[49] Comparisons of the MODIS daily snow albedo product, MOD10A1, with the higher-quality MODIS 16-day albedo product, MCD43C3, are somewhat ambiguous as discussed in the work of *Hall et al.* [2009], and will require much further work to understand. We found generally good correspondence at the lower elevations of the ice sheet and poorer correspondence at the higher elevations between the MOD10A1 and a daily version of MCD43. The relative MOD10A1 albedo values presented in this paper are reasonable and consistent, though the absolute albedo values may not be accurate as compared to the superior MCD43C3 product which is based on more views of the surface [*Schaaf et al.*, 2002]. However, absolute values are not required to draw the conclusions reported herein.

8. Discussion and Conclusions

[50] Researchers use various remote sensing methods to measure melt on the Greenland ice sheet. Each method has advantages and limitations. Algorithms based on active microwave instruments, such as from a scatterometer, are very sensitive to melt and melt extent, and can detect liquid water beneath the ice sheet surface but cannot provide high

spatial resolution and thus great detail, especially in transition areas such as at the snow line. VIS, NIR and IR data provide images of melt at relatively high spatial resolutions (up to 250 m on a daily basis), but cannot image through cloud cover and are not as sensitive to melt as are the microwave sensors. However, when results from these various sensors are combined, or "blended," then the attributes of each are accentuated and the limitations are downplayed.
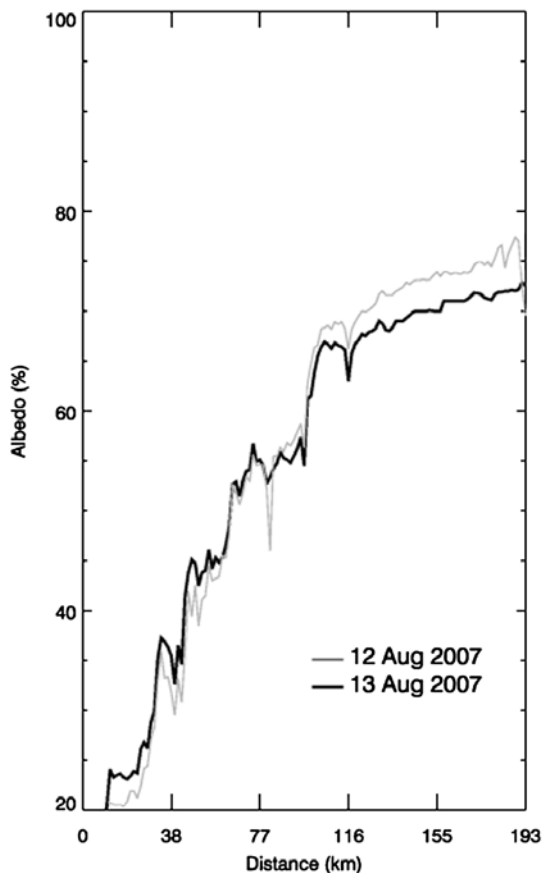
[51] Consistent results from the various products provide confirmation of different melting states on the Greenland ice sheet for the 2007 melt season. Both the MODIS and QS are sensitive to melt onset. The MODIS daily snow albedo product is the most sensitive of the three products for detecting surface changes, but the QS is the most sensitive for detecting liquid water in the surface and near surface of the ice sheet. Surface changes, detected by the MODIS daily snow albedo product, are not necessarily melt related, but may be related to wind effects.

[52] Relative albedo changes seen in the MODIS daily snow albedo product show snow and ice surface changes, including changes in surface melt intensity. The MODIS daily snow albedo product responds to grain size changes between areas with more intense melting (larger grain sizes)
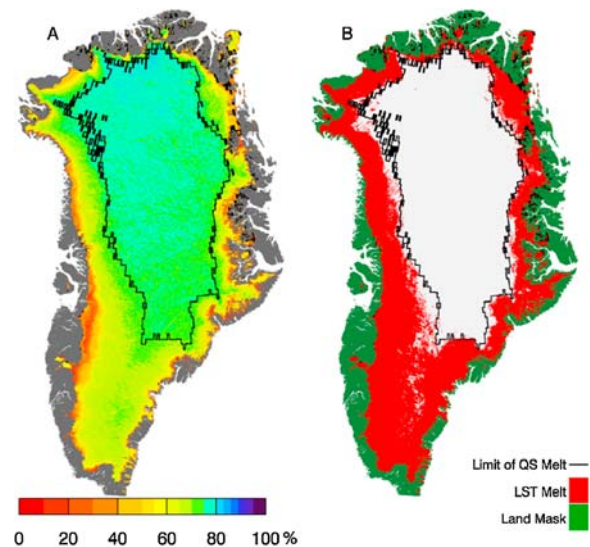
and areas characterized by a frozen surface (smaller grain sizes). Once the grain size has increased due to an earlier melt event, albedo may not regain its highest values after the surface becomes frozen again until new snow is deposited by snow drift or snowfall. This explains much of the albedo variability and spatial patterns in refrozen areas.

[53] Elevation and orientation (surface slope azimuth) play an important role in the melt states of the ice sheet. We did not address orientation in this paper, but using a DEM [*Bamber et al.*, 2001], we show that elevation change can be associated with sudden changes in the state of melting on the ice sheet by causing rapid changes in near-surface air temperature and thus surface temperature. In addition, large or sudden changes in near-surface air temperatures and thus LST can be caused by katabatic winds.

[54] With this suite of melt products from MODIS and QS, we can measure small changes in the surface and near-surface melt states of the snow and ice on the Greenland ice sheet. The products are consistent in identifying physical properties of the complex snowmelt process. The ice sheet responds very quickly to changes in near-surface temperature through surface melting and refreezing and even sometimes by maintaining liquid water just beneath the surface (detected by the QS product), yet the amount and depth of liquid water beneath the surface needs to be evaluated further by in situ observations. Also relevant is

Figure 7. (a) Minimum albedo on a per pixel basis as determined from the MODIS daily snow albedo product, MOD10A1. (b) Total extent of seasonal snowmelt from the MODIS LST and QS melt maps.

a quantitative comparison of the MODIS LST, daily albedo and QS melt maps with melt maps produced using passive microwave data. This is an important follow-up project for future work, not addressed in the present work.

[55] The products provide remarkably consistent results showing the locations of, and sometimes rapid changes in, boundaries between melted versus frozen surface conditions. This work has demonstrated that these are physically meaningful "boundaries" and not artifacts of remote sensing data processing. Using these products, we can improve the precision in mapping surface and near-surface melt on the Greenland ice sheet to enable improved quantification of meltwater runoff.

Figure 6. MOD10A1 albedo plots from 12 to 13 August 2007 showing lowering of albedo from 12 to 13 August where extensive melt on 13 August has caused the albedo to decrease because of grain size increases.

References

Abdalati, W., and K. Steffen (2001), Greenland ice sheet melt extent: 1979–1999, *J. Geophys. Res.*, *106*, 33,983–33,989, doi:10.1029/2001JD900181.

Ackerman, S. A., K. I. Strabala, P. W. P. Menzel, R. A. Frey, C. C. Moeller, and L. E. Gumley (1998), Discriminating clear sky from clouds with MODIS, *J. Geophys. Res.*, *103*, 32,141–32,157, doi:10.1029/1998JD200032.

Bamber, J. L., S. Ekholm, and W. B. Krabill (2001), A new, high-resolution digital elevation model of Greenland fully validated with airborne laser altimeter data, *J. Geophys. Res.*, *106*, 6733–6745, doi:10.1029/2000JB900365.

Barnes, W. L., T. S. Pagano, and V. V. Salomonson (1998), Prelaunch characteristics of the Moderate Resolution Imaging Spectroradiometer

(MODIS) on EOS-AM1, *IEEE Trans. Geosci. Remote Sens.*, *36*, 1088–1100, doi:10.1109/36.700993.

Box, J. E. (2002), Survey of Greenland instrumental temperature records: 1873–2001, *Int. J. Climatol.*, *22*, 1829–1847, doi:10.1002/joc.852.

Box, J. E., and K. Ski (2007), Remote sounding of Greenland supraglacial melt lakes: Implications for subglacial hydraulics, *J. Glaciol.*, *53*, 257–265, doi:10.3189/172756507782202883.

Choudhury, B. J., and A. T. C. Chang (1979), Two-stream theory of reflectance of snow, *IEEE Trans. Geosci. Remote Sens.*, *17*, 63–68.

Comiso, J. C. (2006), Arctic warming signals from satellite observations, *Weather*, *61*(3), 70–76, doi:10.1256/wea.222.05.

Comiso, J., J. Yang, S. Honjo, and R. A. Krishfield (2003), Detection of change in the Arctic using satellite and in situ data, *J. Geophys. Res.*, *108*(C12), 3384, doi:10.1029/2002JC001347.

Dozier, J., S. R. Schneider, and D. F. McGinnis Jr. (1981), Effect of grain size and snowpack water equivalence on visible and near-infrared satellite observations of snow, *Water Resour. Res.*, *17*, 1213–1221, doi:10.1029/WR017i004p01213.

Early, D. S., and D. G. Long (2001), Image reconstruction and enhanced resolution imaging from irregular samples, *IEEE Trans. Geosci. Remote Sens.*, *39*, 291–302, doi:10.1109/36.905237.

Fettweis, X., J.-P. van Ypersele, H. Gallée, F. Lefebre, and W. Lefebre (2007), The 1979–2005 Greenland ice sheet melt extent from passive microwave data using an improved version of the melt retrieval XPGR algorithm, *Geophys. Res. Lett.*, *34*, L05502, doi:10.1029/2006GL028787.

Gregory, J. M., P. Huybrechts, and S. C. B. Raper (2004), Threatened loss of the Greenland ice sheet, *Nature*, *428*, 616, doi:10.1038/428616a.

Greuell, W., J. Kohler, F. Obleitner, P. Glowacki, K. Melvold, E. Bernsen, and J. Oerlemans (2007), Assessment of interannual variations in the surface mass balance of 18 Svalbard glaciers from the Moderate Resolution Imaging Spectroradiometer/Terra albedo product, *J. Geophys. Res.*, *112*, D07105, doi:10.1029/2006JD007245.

Hall, D. K., and G. A. Riggs (2007), Accuracy assessment of the MODIS snow-cover products, *Hydrol. Processes*, *21*, 1534–1547, doi:10.1002/hyp.6715.

Hall, D. K., R. S. Williams Jr., S. B. Luthcke, and N. E. DiGirolamo (2008a), Greenland ice sheet surface temperature, melt and mass loss: 2000–2006, *J. Glaciol.*, *54*, 81–93, doi:10.3189/002214308784409170.

Hall, D. K., J. E. Box, K. A. Casey, S. J. Hook, C. A. Shuman, and K. Steffen (2008b), Comparison of satellite-derived and in-situ observations of ice and snow surface temperatures over Greenland, *Remote Sens. Environ.*, *112*, 3739–3749, doi:10.1016/j.rse.2008.05.007.

Hall, D. K., C. B. Schaaf, Z. Wang, and G. A. Riggs (2009), Enhancement of the MODIS daily snow albedo product, paper presented at 89th Annual Meeting, Am. Meteorol. Soc., Phoenix, Ariz., 11–15 Jan.

Hanna, E., P. Huybrechts, K. Steffen, J. Cappelen, R. Huff, C. Shuman, T. Irvine-Fynn, S. Wise, and M. Griffiths (2008), Increased runoff from melt from the Greenland ice sheet: A response to global warming, *J. Clim.*, *21*, 331–341, doi:10.1175/2007JCLI1964.1.

Hoffman, M. J., A. G. Fountain, and G. E. Liston (2008), Surface energy balance and melt thresholds over 11 years at Taylor Glacier, Antarctica, *J. Geophys. Res.*, *113*, F04014, doi:10.1029/2008JF001029.

Hook, S. J., R. G. Vaughan, H. Tonooka, and S. G. Schladow (2007), Absolute radiometric in-flight validation of mid infrared and thermal infrared data from ASTER and MODIS on the Terra spacecraft using the Lake Tahoe, CA/NV, USA, automated validation site, *IEEE Trans. Geosci. Remote Sens.*, *45*, 1798–1807, doi:10.1109/TGRS.2007.894564.

Hori, M., et al. (2006), In-situ measured spectral directional emissivity of snow and ice in the 8–14 μm atmospheric window, *Remote Sens. Environ.*, *100*, 486–502, doi:10.1016/j.rse.2005.11.001.

Jet Propulsion Laboratory (2006), QuikSCAT Science Data Product User's Manual, *Doc. D-18053-RevA*, 90 pp., Pasadena, Calif. (Available at ftp://podaac.jpl.nasa.gov/ocean_wind/quikscat/L2B/doc/QSUG_v3.pdf)

Key, J., and M. Haefliger (1992), Arctic ice surface temperature retrieval from AVHRR thermal channels, *J. Geophys. Res.*, *97*, 5885–5893.

Klein, A. G., and J. Stroeve (2002), Development and validation of a snow albedo algorithm for the MODIS instrument, *Ann. Glaciol.*, *34*, 45–52, doi:10.3189/172756402781817662.

Klein, L. A., and C. Swift (1977), An improved model for the dielectric constant of sea water at microwave frequencies, *IEEE Trans. Antennas Propag.*, *25*(1), 104–111, doi:10.1109/TAP.1977.1141539.

Krabill, W., et al. (2004), Greenland ice sheet: Increased coastal thinning, *Geophys. Res. Lett.*, *31*, L24402, doi:10.1029/2004GL021533.

Liang, S. (2001), Narrow to broadband conversion of land surface albedo I: Algorithms, *Remote Sens. Environ.*, *76*, 213–238, doi:10.1016/S0034-4257(00)00205-4.

Lucht, W., and P. Lewis (2000), Theoretical noise sensitivity of BRDF and albedo retrieval from the EOS-MODIS and MISR sensors with respect to angular sampling, *Int. J. Remote Sens.*, *21*, 81–98, doi:10.1080/014311600211000.

Luthcke, S. B., H. J. Zwally, W. Abdalati, D. D. Rowlands, R. D. Ray, R. S. Nerem, F. G. Lemoine, J. J. McCarthy, and D. S. Chinn (2006), Recent Greenland ice mass loss by drainage system from satellite gravity observations, *Science*, *314*(5803), 1286–1289, doi:10.1126/science.1130776.

Mernild, S. H., G. E. Liston, C. A. Hiemstra, and K. Steffen (2009), Record 2007 Greenland ice sheet melt extent and runoff, *Eos Trans. AGU*, *90*(2), 13–14, doi:10.1029/2009EO020002.

Mote, T. (2007), Greenland surface melt trends 1973–2007: Evidence of a large increase in 2007, *Geophys. Res. Lett.*, *34*, L22507, doi:10.1029/2007GL031976.

Mote, T. L., and M. R. Anderson (1995), Variations in snowpack melt on the Greenland ice sheet, based on passive-microwave measurements, *J. Glaciol.*, *41*, 51–60.

Nghiem, S. V., and W. Y. Tsai (2001), Global snow cover monitoring with spaceborne Ku-band scatterometer, *IEEE Trans. Geosci. Remote Sens.*, *39*, 2118–2134, doi:10.1109/36.957275.

Nghiem, S. V., R. Kwok, S. H. Yueh, J. A. Kong, M. A. Tassoudji, C. C. Hsu, and R. T. Shin (1995), Polarimetric scattering from layered media with multiple species of scatterers, *Radio Sci.*, *30*(4), 835–852, doi:10.1029/95RS01247.

Nghiem, S., K. Steffen, R. Kwok, and W.-Y. Tsai (2001), Detection of snowmelt regions on the Greenland ice sheet using diurnal backscatter change, *J. Glaciol.*, *47*, 539–547, doi:10.3189/172756501781831738.

Nghiem, S. V., K. Steffen, G. Neumann, and R. Huff (2005), Mapping of ice layer extent and snow accumulation in the percolation zone of the Greenland ice sheet, *J. Geophys. Res.*, *110*, F02017, doi:10.1029/2004JF000234.

Nolin, A. W., and S. Liang (2000), Progress in bi-directional reflectance modeling and applications for surface particulate media: Snow and soils, *Remote Sens. Rev.*, *18*, 307–342.

Nolin, A. W., and M. C. Payne (2007), Classification of glacier zones in western Greenland using albedo and surface roughness from Multi-angle Imaging SpectroRadiometer (MISR), *Remote Sens. Environ.*, *107*, 264–275, doi:10/1016/j.rse.2006.11.004.

Nolin, A. W., and J. C. Stroeve (1997), The changing albedo of the Greenland ice sheet: Implications for climate change, *Ann. Glaciol.*, *25*, 51–57.

Platnick, S., M. D. King, S. A. Ackerman, W. P. Menzel, B. A. Baum, J. C. Riédi, and R. A. Frey (2003), The MODIS cloud products: Algorithms and examples from Terra, *IEEE Trans. Geosci. Remote Sens.*, *41*, 459–473, doi:10.1109/TGRS.2002.808301.

Rignot, E., J. E. Box, E. Burgess, and E. Hanna (2008), Mass balance of the Greenland ice sheet from 1958 to 2007, *Geophys. Res. Lett.*, *35*, L20502, doi:10.1029/2008GL035417.

Salisbury, J. W., D. M. D'Aria, and A. Wald (1994), Measurements of thermal infrared spectral reflectance of frost, snow, and ice, *J. Geophys. Res.*, *99*, 24,235–24,240, doi:10.1029/94JB00579.

Schaaf, C. B., et al. (2002), First operational BRDF, albedo nadir reflectance products from MODIS, *Remote Sens. Environ.*, *83*, 135–148, doi:10.1016/S0034-4257(02)00091-3.

Schaaf, C., J. Martonchik, B. Pinty, Y. Govaerts, F. Gao, A. Lattanzio, J. Liu, A. Strahler, and M. Taberner (2008), Retrieval of surface albedo from satellite sensors, in *Advances in Land Remote Sensing: System, Modelling, Inversion and Application*, edited by S. Liang, pp. 219–244, Springer, New York.

Serreze, M. C., J. E. Walsh, F. S. Chapin III, T. Osterkamp, M. Dyurgerov, V. Romanovsky, W. C. Oechel, J. Morison, T. Zhang, and R. G. Barry (2000), Observational evidence of recent change in the northern high-latitude environment, *Clim. Change*, *46*, 159–207, doi:10.1023/A:1005504031923.

Sharp, M., and L. Wang (2009), A five-year record of summer melt on Eurasian Arctic ice caps, *J. Clim.*, *22*, 133–145, doi:10.1175/2008JCLI2425.1.

Sneed, W. A., and G. S. Hamilton (2007), Evolution of melt pond volume on the surface of the Greenland ice sheet, *Geophys. Res. Lett.*, *34*, L03501, doi:10.1029/2006GL028697.

Sorman, A. U., Z. Akyurek, A. Sensoy, A. A. Sorman, and A. E. Tekeli (2006), Commentary on comparison of MODIS snow cover and albedo products with ground observations over the mountainous terrain of Turkey, *Hydrol. Earth Syst. Sci. Discuss.*, *3*, 3655–3673.

Stamnes, K., S.-C. Tsay, W. Wiscombe, and K. Jayaweera (1988), Numerically stable algorithm for discrete-ordinate-method radiative transfer in multiple scattering and emitting layered media, *Appl. Opt.*, *27*, 2502–2509, doi:10.1364/AO.27.002502.

Steffen, K., and J. Box (2001), Surface climatology of the Greenland ice sheet: Greenland climate network 1995–1999, *J. Geophys. Res.*, *106*, 33,951–33,964, doi:10.1029/2001JD900161.

Steffen, K., S. V. Nghiem, R. Huff, and G. Neumann (2004), The melt anomaly of 2002 on the Greenland ice sheet from active and passive microwave satellite observations, *Geophys. Res. Lett.*, *31*, L20402, doi:10.1029/2004GL020444.

Stroeve, J., and K. Steffen (1998), Variability of AVHRR-derived clear-sky surface temperature over the Greenland ice sheet, *J. Appl. Meteorol.*, *37*, 23–31, doi:10.1175/1520-0450(1998)037<0023:VOADCS>2.0.CO;2.

Stroeve, J., M. Haefliger, and K. Steffen (1996), Surface temperature from ERS-1 ATSR infrared thermal satellite data in polar regions, *J. Appl. Meteorol.*, *35*, 1231–1239, doi:10.1175/1520-0450(1996)035<1231:STFAIT>2.0.CO;2.

Stroeve, J. C., A. W. Nolin, and K. Steffen (1997), Comparison of AVHRR-derived and in situ surface albedo over the Greenland ice sheet, *Remote Sens. Environ.*, *62*, 262–276, doi:10.1016/S0034-4257(97)00107-7.

Stroeve, J. C., J. Box, J. Gao, S. Liang, A. Nolin, and C. Schaaf (2005), Accuracy assessment of the MODIS 16-day snow albedo product: Comparisons with Greenland in situ measurements, *Remote Sens. Environ.*, *94*, 46–60, doi:10.1016/j.rse.2004.09.001.

Stroeve, J., J. Box, and T. Haran (2006), Evaluation of the MODIS (MOD10A) daily snow albedo product over the Greenland ice sheet, *Remote Sens. Environ.*, *105*, 155–171, doi:10/1016/j.rse.2006.06.009.

Strugnell, N. C., and W. Lucht (2001), Continental-scale albedo inferred from AVHRR data, land cover class and field observations of typical BRDFs, *J. Clim.*, *14*, 1360–1376, doi:10.1175/1520-0442(2001)014<1360:AATICS>2.0.CO;2.

Tedesco, M. (2007), Snowmelt detection over the Greenland ice sheet from SSM/I brightness temperature daily variations, *Geophys. Res. Lett.*, *34*, L02504, doi:10.1029/2006GL028466.

Tedesco, M., M. Serreze, and X. Fettweis (2008), Diagnosing the extreme surface melt event over southwestern Greenland in 2007, *Cryosphere*, *2*, 159–166.

Tekeli, A. E., A. Ensoy, A. Sorman, Z. Akyürek, and Ü. Sorman (2006), Accuracy assessment of MODIS daily snow albedo retrievals with *in situ* measurements in Karasu basin, Turkey, *Hydrol. Processes*, *20*, 705–721, doi:10.1002/hyp.6114.

Tiuri, M. E., A. H. Sihvola, E. G. Nyfors, and M. T. Hallikainen (1984), The complex dielectric constant of snow at microwave frequencies, *IEEE J. Oceanic Eng.*, *9*(5), 377–382, doi:10.1109/JOE.1984.1145645.

Tsang, L., J. A. Kong, and R. T. Shin (1985), *Theory of Microwave Remote Sensing*, John Wiley, New York.

Ulaby, F. T., R. K. Moore, and A. K. Fung (1981), *Microwave Remote Sensing: Active and Passive*, Artech House, Reading, Mass.

van den Broeke, M., P. Smeets, J. Ettema, C. van der Veen, R. van de Wal, and J. Oerlemans (2008), Partitioning of energy and meltwater fluxes in the ablation zone of the west Greenland ice sheet, *Cryosphere*, *2*, 179–189.

van de Wal, R. S. W., W. Greuell, M. R. van den Broeke, C. H. Reijmer, and J. Oerlemans (2005), Surface mass balance observations and automatic weather station data along a transect near Kangerlussuaq, west Greenland, *Ann. Glaciol.*, *42*, 311–316, doi:10.3189/172756405781812529.

Wald, A. (1994), Modeling thermal infrared (2–14 μm) reflectance spectra of frost and snow, *J. Geophys. Res.*, *99*, 24,241–24,250, doi:10.1029/94JB01560.

Wan, Z. (2008), New refinements and validation of the MODIS land-surface temperature/emissivity products, *Remote Sens. Environ.*, *112*, 59–74, doi:10.1016/j.rse.2006.06.026.

Wan, Z., Y. Zhang, Q. Zhang, and Z.-L. Li (2002), Validation of the land-surface temperature products retrieved from Terra Moderate Resolution Imaging Spectroradiometer data, *Remote Sens. Environ.*, *83*, 163–180, doi:10.1016/S0034-4257(02)00093-7.

Wang, L., M. Sharp, B. Rivard, and K. Steffen (2007), Melt season duration and ice layer formation on the Greenland ice sheet, 2000–2004, *J. Geophys. Res.*, *112*, F04013, doi:10.1029/2007JF000760.

Wang, X., and J. Key (2003), Recent trends in Arctic surface, cloud, and radiation properties from space, *Science*, *299*(5613), 1725–1728, doi:10.1126/science.1078065.

Wang, X., and J. Key (2005), Arctic surface, cloud, and radiation properties based on the AVHRR Polar Pathfinder data set. Part II: Recent trends, *J. Clim.*, *18*, 2575–2593, doi:10.1175/JCLI3439.1.

Wismann, V. (2000), Monitoring of seasonal snowmelt on Greenland with ERS Scatterometer data, *IEEE Trans. Geosci. Remote Sens.*, *38*, 1821–1826, doi:10.1109/36.851766.

Zwally, H. J., M. B. Giovinetto, J. Li, H. G. Cornejo, M. A. Beckley, A. C. Brenner, J. L. Saba, and D. Yi (2005), Mass changes of the Greenland and Antarctic ice sheets and shelves and contributions to sea-level rise: 1992–2002, *J. Glaciol.*, *51*, 509–527, doi:10.3189/172756505781829007.

N. E. DiGirolamo, Science Systems and Applications, Inc., 10210 Greenbelt Road, Suite 600, Lanham, MD 20706, USA.

D. K. Hall, Cryospheric Sciences Branch, Code 614.1, NASA Goddard Space Flight Center, Greenbelt, MD 20771, USA. (dorothy.k.hall@nasa.gov)

G. Neumann and S. V. Nghiem, Jet Propulsion Laboratory, California Institute of Technology, Pasadena, CA 91109, USA.

C. B. Schaaf, Department of Geography and Center for Remote Sensing, Boston University, Boston, MA 02215, USA.